New Journal of Physics
The open access journal for physics

Scattering of coherent states on a single artificial atom

B Peropadre[1,3], J Lindkvist[2,3], I-C Hoi[2], C M Wilson[2], J J Garcia-Ripoll[1], P Delsing[2] and G Johansson[2,4]

[1] Instituto de Física Fundamental, CSIC, Calle Serrano 113-bis, Madrid E-28006, Spain

[2] Department of Microtechnology and Nanoscience, Chalmers University of Technology, Göteborg, Sweden

E-mail: Goran.L.Johansson@chalmers.se

New Journal of Physics **15** (2013) 035009 (17pp)
Received 5 October 2012
Published 6 March 2013
Online at http://www.njp.org/
doi:10.1088/1367-2630/15/3/035009

Abstract. In this work, we theoretically analyze a circuit quantum electrodynamics design where propagating quantum microwaves interact with a single artificial atom, a single Cooper-pair box. In particular, we derive a master equation in the so-called transmon regime, including coherent drives. Inspired by recent experiments, we then apply the master equation to describe the dynamics in both a two-level and a three-level approximation of the atom. In the two-level case, we also discuss how to measure photon antibunching in the reflected field and how it is affected by finite temperature and finite detection bandwidth.

[3] These two authors contributed equally to the manuscript.

[4] Author to whom any correspondence should be addressed.

Contents

1. Introduction

In recent years, the field of circuit quantum electrodynamics (circuit QED) [1, 2] has become one of the most promising platforms in the study of light–matter interaction. One of the most important breakthroughs in this field was the achievement of a strong coupling between light and matter, or microwave photons and Josephson-based artificial atoms [3, 4]. Since then, many experiments have been carried out within the framework of superconducting circuits [5–9], revealing a wide variety of novel quantum phenomena. Most of these experiments share a common feature, namely the interaction between artificial atoms and isolated modes of the electromagnetic field in a cavity. Within circuit QED, there is now growing interest in studying propagating fields interacting with artificial atoms, owing to, e.g., its potential interest for condensed matter [10] and all-optical quantum information [11]. Theoretically, coherent coupling between an atom or superconducting qubit and a one-dimensional continuum of modes has been discussed for some time [12–17], and there exist now a growing number of experiments investigating this system in a circuit QED setup [18–25].

In this paper, we report on an in-depth microscopic description of the coherent coupling between a field propagating through an open transmission line (TL) and a superconducting artificial atom based on the single Cooper-pair box (SCB) [26–32]. In more detail, we analyze the so-called transmon regime [8, 33] and study the photon transport properties of this system according to different approximations. On the one hand, in the two-level approximation and under certain conditions, the qubit behaves like a saturable mirror [12, 13]. On the other hand, by including a second excited state of the transmon, we can effectively make the medium transparent for the incident photons using a coherent control field in resonance with this second transition. Finally, we also discuss how the photon antibunching observed in the reflected field is reduced by finite temperature and finite detection bandwidth. Our theoretical predictions are in full agreement with recent experiments [22, 23, 25].

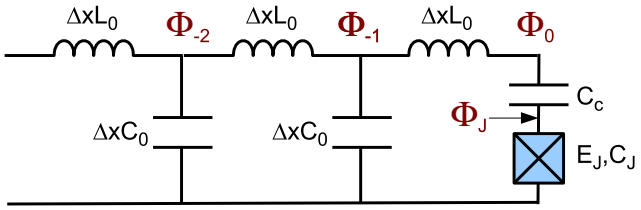

Figure 1. Discretized circuit describing the interaction of an SCB with microwaves photons propagating in a semi-infinite TL.

This paper is organized as follows. In section 2, we derive the master equation of an SCB coupled to an open TL. In section 2.1, we start from a discretized lumped-element description of the TL and in section 2.2 we proceed to the continuum description. In section 2.3, we discuss the regime where the system can be described as an SCB weakly coupled to the voltage of the TL, at the coupling point. We thus arrive at the Hamiltonian of a voltage-biased SCB, weakly coupled to a bath of harmonic oscillators, i.e. the electromagnetic modes of the TL. Making standard weak coupling approximations, we then derive a master equation in Lindblad form in section 2.4 and attach a coherent drive in section 2.5. For simplicity, we go through these derivations considering an SCB at the end of a semi-infinite TL, but in section 2.6 we discuss how the master equation can be straightforwardly extended to an arbitrary number of semi-inifinte TLs, all meeting at the SCB. In particular, this includes the important case of a single infinite TL.

In section 3, we then apply the master equation to a few experimentally relevant cases [22, 23]. Section 3.1 is devoted to the reflection and transmission of a single near resonant coherent drive, while section 3.2 includes two coherent drives, where one is used to control the transmission of the other. Finally in section 3.3, we investigate how the photon antibunching observed in the reflected field is influenced by finite temperature and finite detection bandwidth.

2. The model

In this section, we present a general formalism of the light–matter scattering in a one-dimensional continuum from a microscopic point of view. We start from a Hamiltonian description, arriving at the well-known input–output relations for the microwave field. We then follow the usual approach [34] to describe the joint state of the light–matter system by introducing dissipation, resulting in the standard quantum optical master equation.

2.1. The discrete circuit model, Hamiltonian and equations of motion

Consider a semi-infinite TL with characteristic inductance L_0 and capacitance C_0 per unit length. We discretize the TL [35] in units of the small length Δx, which we take to zero at the end of the calculation. The TL nodes are numbered with negative integers, while the SCB island node has index J and its Josephson junction has a capacitance C_J to ground and a Josephson energy E_J. The SCB is coupled to the TL at the zeroth node, through the capacitance C_c, as depicted in figure 1.

To describe the circuit dynamics, we use the node fluxes $\Phi_\alpha(t) = \int^t \mathrm{d}t' V_\alpha(t')$ as coordinates [36]. They are the time integrals of the node voltages and although less intuitive than

the voltages, this choice greatly simplifies the description of the Josephson junction. Starting from a circuit Lagrangian, we can derive the discrete circuit Hamiltonian [37]

$$H_{\mathrm{d}} = \frac{(p_0 + p_{\mathrm{J}})^2}{2C_{\mathrm{J}}} + \frac{p_0^2}{2C_{\mathrm{c}}} - E_{\mathrm{J}} \cos\left(\frac{2e}{\hbar}\Phi_{\mathrm{J}}\right) + \frac{1}{\Delta x}\sum_{n<0}\frac{p_n^2}{2C_0} + \frac{(\Phi_{n+1} - \Phi_n)^2}{2L_0}, \tag{1}$$

where the charges p_α are the conjugate momenta to the node fluxes Φ_α, fulfilling the canonical commutation relations

$$[\Phi_\alpha, p_\beta] = \mathrm{i}\hbar\delta_{\alpha,\beta}, \quad [\Phi_\alpha, \Phi_\beta] = [p_\alpha, p_\beta] = 0,$$

where $\delta_{\alpha,\beta}$ denotes Kronecker's delta. From the Hamiltonian, we obtain Heisenberg's equations of motion for the TL operators ($n < 0$)

$$\partial_t \Phi_n = \frac{p_n}{\Delta x C_0}, \quad \partial_t p_n = \frac{\Phi_{n-1} - 2\Phi_n + \Phi_{n+1}}{\Delta x L_0} \tag{2}$$

and for the SCB operators

$$\partial_t p_0 = \frac{\Phi_{-1} - \Phi_0}{\Delta x L_0}, \tag{3}$$

$$\partial_t \Phi_0 = \frac{p_0 + p_{\mathrm{J}}}{C_{\mathrm{J}}} + \frac{p_0}{C_{\mathrm{c}}} = \frac{C_\Sigma}{C_{\mathrm{c}} C_{\mathrm{J}}} p_0 + \frac{p_{\mathrm{J}}}{C_{\mathrm{J}}}, \tag{4}$$

$$\partial_t p_{\mathrm{J}} = -E_{\mathrm{J}}\frac{2e}{\hbar}\sin\left(\frac{2e}{\hbar}\Phi_{\mathrm{J}}\right), \tag{5}$$

$$\partial_t \Phi_{\mathrm{J}} = \frac{p_0 + p_{\mathrm{J}}}{C_{\mathrm{J}}}, \tag{6}$$

where $C_\Sigma = C_{\mathrm{c}} + C_{\mathrm{J}}$.

2.2. Continuum limit

In the continuum limit $\Delta x \to 0$, the charge of each TL node will go to zero together with the node capacitance. Thus, we define a charge density field $p(x_n, t) = p_n(t)/\Delta x$ and a flux field $\Phi(x_n, t) = \Phi_n(t)$, where we define the spatial coordinate $x_n = n\Delta x$ for $n < 0$, along the TL. The continuum equations of motion for the TL ($x < 0$) are

$$\partial_t p(x) = \frac{\partial_x^2 \Phi(x)}{L_0}, \quad \partial_t \Phi(x) = \frac{p(x)}{C_0}. \tag{7}$$

These are the equations of motion for the massless Klein–Gordon field, having freely propagating left- and right- moving solutions with velocity $v = 1/\sqrt{L_0 C_0}$. Therefore, we can write the general solution for $x < 0$ as a linear combination of right- and left- moving second-quantized fields

$$\begin{aligned}
\Phi_{\rightleftarrows}(x, t) &= \sqrt{\frac{\hbar Z_0}{4\pi}}\int_0^\infty \frac{\mathrm{d}\omega}{\sqrt{\omega}}\left(a_\omega^{\rightleftarrows} \mathrm{e}^{-\mathrm{i}(\omega t \mp k_\omega x)} + \mathrm{h.c.}\right), \\
p_{\rightleftarrows}(x, t) &= -\mathrm{i}\sqrt{\frac{\hbar Z_0}{4\pi}}\int_0^\infty \mathrm{d}\omega\sqrt{\omega}\left(a_\omega^{\rightleftarrows} \mathrm{e}^{-\mathrm{i}(\omega t \mp k_\omega x)} - \mathrm{h.c.}\right),
\end{aligned} \tag{8}$$

where $k_\omega = \omega/v$ and $Z_0 = \sqrt{L_0/C_0}$ is the characteristic impedance of the TL. The operators $a_\omega^{\leftrightarrows}$ annihilate a left/right-moving photon with frequency ω, and obey the bosonic canonical commutation relations, $[a_\omega^{\leftarrow}, (a_{\omega'}^{\leftarrow})^\dagger] = [a_\omega^{\rightarrow}, (a_{\omega'}^{\rightarrow})^\dagger] = \delta(\omega - \omega')$ and $[a_\omega^{\leftarrow}, (a_{\omega'}^{\rightarrow})^\dagger] = [a_\omega^{\rightleftarrows}, a_{\omega'}^{\rightleftarrows}] = 0$. Finally, we note that in the continuum limit, (3) changes into

$$\partial_t p_0 = -\frac{\partial_x \Phi(0^-)}{L_0}. \tag{9}$$

To describe the system dynamics, we first need to specify the incoming, right-moving field

$$\Phi^{\text{in}}(t) = \Phi_{\rightarrow}(0^-, t).$$

Given this initial condition, we can then calculate the SCB dynamics, as well as the outgoing field

$$\Phi^{\text{out}}(t) = \Phi_{\leftarrow}(0^-, t),$$

propagating to the left in the line. The flux at $x = 0$ is simply the sum of the incoming and outgoing flux fields

$$\Phi_0(t) = \Phi(0^-, t) = \Phi^{\text{in}}(t) + \Phi^{\text{out}}(t) + V_{\text{dc}} t, \tag{10}$$

where for simplicity we also explicitly extracted the dc voltage bias V_{dc}, implying that Φ^{in} and Φ^{out} have no dc components. Now, solving for p_0 from (4) gives

$$p_0 = \frac{C_c C_J}{C_\Sigma}\left[V_{\text{dc}} + \partial_t(\Phi^{\text{in}} + \Phi^{\text{out}})\right] - \frac{C_c}{C_\Sigma} p_J \tag{11}$$

and inserting this expression into (6), we arrive at

$$\partial_t \Phi_J = \frac{p_J + C_c\left[V_{\text{dc}} + \partial_t(\Phi^{\text{in}} + \Phi^{\text{out}})\right]}{C_\Sigma}. \tag{12}$$

We then insert Φ_0 from (10) in (13) and arrive at

$$\partial_t p_0 = -\frac{\partial_x \Phi(0^-)}{L_0} = \frac{\partial_t(\Phi^{\text{in}} - \Phi^{\text{out}})}{Z_0}, \tag{13}$$

where we used the relation $\partial_x \Phi_{\rightleftarrows}(0^-) = \mp v^{-1} \partial_t \Phi_{\rightleftarrows}(0^-)$ to change the spatial derivative into a time derivative. Inserting the expression for p_0 from (11) into the left-hand side of this equation and integrating once with respect to time leads to

$$\Phi^{\text{out}} = \Phi^{\text{in}} + Z_0 \frac{C_c}{C_\Sigma} p_J - \tau_{\text{RC}} \partial_t(\Phi^{\text{in}} + \Phi^{\text{out}}), \tag{14}$$

where the time $\tau_{\text{RC}} = C_c C_J Z_0 / C_\Sigma$ is the characteristic RC time for discharging the SCB through the TL. Equations (5), (12) and (14), in principle, give the full time evolution of the SCB operators Φ_J and p_J as well as the out-field, in terms of the in-field. However, to solve these nonlinear equations straightforwardly, we need to make some approximations.

2.3. Voltage-biased single Cooper-pair box approximation

In the following, we will neglect the last term in (14). Since the time derivative enters the product with τ_{RC}, this will be a good approximation as long as the relevant frequencies of the incoming field Φ^{in} and of the SCB dynamics (p_{J}) are much lower than the inverse RC time. Under this approximation, the final equations of motion are

$$\partial_t \Phi_{\mathrm{J}} = \frac{p_{\mathrm{J}} + C_{\mathrm{c}}\left(V_{\mathrm{dc}} + 2\partial_t \Phi^{\mathrm{in}} + \frac{\tau_{\mathrm{RC}}}{C_{\mathrm{J}}}\partial_t p_{\mathrm{J}}\right)}{C_\Sigma}, \tag{15}$$

$$\partial_t p_{\mathrm{J}} = -E_{\mathrm{J}}\frac{2e}{\hbar}\sin\left(\frac{2e}{\hbar}\Phi_{\mathrm{J}}\right), \tag{16}$$

$$\Phi^{\mathrm{out}} = \Phi^{\mathrm{in}} + \frac{\tau_{\mathrm{RC}}}{C_{\mathrm{J}}} p_{\mathrm{J}}. \tag{17}$$

Here we also note that this approximation is valid in recent experiments [22, 23], where $Z_0 = 50\,\Omega$, $C_{\mathrm{c}} \sim 10\,\mathrm{fF}$ and $C_{\mathrm{J}} \sim 25\,\mathrm{fF}$, giving an inverse RC timescale of $1/(2\pi\tau_{\mathrm{RC}}) \sim 400\,\mathrm{GHz}$, which is around 50 times higher than the relevant frequency of Φ^{in} and p_{J}, set by the qubit frequency $\sim$7.5 GHz.

The above set of equations (15)–(17) corresponds to the Hamiltonian

$$H = H_{\mathrm{sys}} + H_{\mathrm{int}} + H_{\mathrm{bath}}, \tag{18}$$

$$H_{\mathrm{sys}} = \frac{[p_{\mathrm{J}} + C_{\mathrm{c}}V_{\mathrm{dc}}]^2}{2C_\Sigma} - E_{\mathrm{J}}\cos\left(\frac{2e}{\hbar}\Phi_{\mathrm{J}}\right), \tag{19}$$

$$H_{\mathrm{int}} = \frac{C_{\mathrm{c}}}{C_\Sigma}(p_{\mathrm{J}} + C_{\mathrm{c}}V_{\mathrm{dc}})\partial_t\Phi(0^-, t), \tag{20}$$

$$H_{\mathrm{bath}} = \frac{\left[C_{\mathrm{c}}\partial_t\Phi(0^-, t)\right]^2}{2C_\Sigma} + \int_{-\infty}^{0}\frac{p(x,t)^2}{2C_0} + \frac{[\partial_x\Phi(x,t)]^2}{2L_0}\,\mathrm{d}x. \tag{21}$$

Thus, we have arrived at the Hamiltonian of a voltage-biased SCB, weakly coupled to the TL voltage at $x = 0$, i.e. $V_0(t) = \partial_t\Phi_0(t)$. (Here, we note that for the uncoupled TL, without SCB, $\Phi_0(t) = 2\Phi^{\mathrm{in}}(t)$ due to the perfect reflection.) Truncating the Hilbert space of H_{sys} to two levels, (18) is just the spin-boson Hamiltonian. From this point, we can proceed with a Bloch–Redfield derivation of a master equation for the SCB only [38]. By comparing to section 3.2 in [34], we also note that the equations of motion (15)–(16) can be interpreted as quantum Langevin equations (QLE) of the form

$$\dot{Y} = \frac{\mathrm{i}}{\hbar}[H_{\mathrm{sys}}, Y] + \frac{\mathrm{i}}{2\hbar}[\gamma\dot{X} - 2\sqrt{\gamma v}\dot{A}^{\mathrm{in}}, [X, Y]]_+, \tag{22}$$

whereas (17) stands for the input–output relation

$$A^{\mathrm{out}}(t) = A^{\mathrm{in}}(t) - \sqrt{\frac{\gamma}{v}}X(t) \tag{23}$$

using the identifications $Y = \Phi_{\mathrm{J}}$, $X = -(p_{\mathrm{J}} + C_{\mathrm{c}}V_{\mathrm{dc}})$, $A^{\mathrm{in}} = \sqrt{C_0}\Phi^{\mathrm{in}}$ and where

$$\gamma = Z_0\left(\frac{C_{\mathrm{c}}}{C_\Sigma}\right)^2 \tag{24}$$

is the damping constant that accounts for spontaneous emission.

2.4. Master equation

From the QLE (22), we can derive a master equation for the reduced density matrix of the SCB in the transmon regime. As the input field, we first consider a thermal background at temperature T, giving rise to a photon occupation number of

$$n_\omega = \frac{1}{\exp(\hbar\omega/k_{\rm B}T) - 1}. \tag{25}$$

We assume that the density matrix initially can be written as a direct product, as well as Markovian properties and short correlation times for the TL variables. In the case when the damping (24) is much smaller than the system eigenenergies, we arrive, after also employing the rotating wave approximation, at the following quantum optical master equation,

$$\dot\rho(t) = -\frac{\rm i}{\hbar}[H_{\rm sys}, \rho] + \frac{2\gamma}{\hbar}\sum_m \omega_m[(n_{\omega_m}+1)\mathcal{D}(X_m^-)\rho + n_{\omega_m}\mathcal{D}(X_m^+)\rho] \tag{26}$$

with the Lindblad operator defined by $\mathcal{D}(c)\rho = c\rho c^\dagger - \frac{1}{2}\left(c^\dagger c\rho + \rho c^\dagger c\right)$. Also, X has been decomposed into eigenoperators of $H_{\rm sys}$,

$$\left[H_{\rm sys}, X_m^\pm\right] = \pm\hbar\omega_m X_m^\pm, \quad \omega_m > 0, \tag{27}$$

which is always possible as long as the eigenstates of $H_{\rm sys}$ form a complete set.

Projecting the master equation onto the SCB eigenstates $|i\rangle$, $H_{\rm sys}|i\rangle = \omega_i|i\rangle$ ($i \in \{0, 1, 2, \ldots\}$), we arrive at the following equation for the diagonal elements,

$$\dot\rho_{ii} = \sum_{j\neq i}\Gamma_{ji}\rho_{jj} - \Gamma_{ij}\rho_{ii}, \tag{28}$$

where the relaxation ($\omega_{ij} = \omega_i - \omega_{\rm J} > 0$) rates are

$$\Gamma_{ij} = \frac{2\gamma}{\hbar}\omega_{ij}\left(1 + n_{\omega_{ij}}\right)|\langle i|X|j\rangle|^2 \tag{29}$$

and the excitation ($\omega_{ij} < 0$) rates are

$$\Gamma_{ij} = \frac{2\gamma}{\hbar}|\omega_{ij}|n_{\omega_{ij}}|\langle i|X|j\rangle|^2. \tag{30}$$

Noting that $X = -(p_{\rm J} + C_{\rm c}V_{\rm dc})$ is the charge operator, the matrix elements can be calculated numerically from the SCB Hamiltonian in (19). Denoting the SCB charging energy by $E_{\rm C} = e^2/2C_\Sigma$, the transmon regime is found for $E_{\rm J} \gg E_{\rm C}$ [33]. Here, the SCB spectrum approaches a linear oscillator with the junction plasma frequency $\omega_{\rm p} = \sqrt{8E_{\rm J}E_{\rm C}}/\hbar$, and the charge operator asymptotically couples only neighboring eigenstates [33]. We find the non-zero relaxation rates

$$\Gamma_{(j+1)j} = \pi(j+1)\kappa^2\frac{E_{\rm J}}{\hbar}\frac{Z_0}{R_K}(1 + n_{\omega_{\rm p}}) \tag{31}$$

and excitation rates

$$\Gamma_{j(j+1)} = \pi(j+1)\kappa^2\frac{E_{\rm J}}{\hbar}\frac{Z_0}{R_K}n_{\omega_{\rm p}}, \tag{32}$$

where $R_K = h/e^2 \approx 25\,\mathrm{k}\,\Omega$ denotes the quantum of resistance. The off-diagonal ($i \neq j$) elements are subject to a pure exponential decay,

$$\dot{\rho}_{ij} = -\gamma_{ij}\rho_{ij} \tag{33}$$

with dephasing rates

$$\gamma_{ij} = \Gamma_\phi^i + \Gamma_\phi^j + \frac{1}{2}\left(\sum_{k\neq i}\Gamma_{ik} + \sum_{k\neq j}\Gamma_{jk}\right), \tag{34}$$

equal to half the sum of all rates for transitions from states $|i\rangle$ and $|j\rangle$, as well as the pure dephasing rates

$$\Gamma_\phi^k = \frac{2\gamma}{\hbar}\frac{k_\mathrm{B}T}{\hbar}|\langle k|X|k\rangle|^2. \tag{35}$$

The pure dephasing rates depend on the dc voltage, through the SCB spectrum, according to

$$|\langle k|X|k\rangle| = \frac{e}{4E_\mathrm{C}}\left|\frac{\partial\omega_k(n_\mathrm{g})}{\partial n_\mathrm{g}}\right|, \tag{36}$$

where $n_\mathrm{g} = C_\mathrm{c}V_\mathrm{dc}/2e$ is the dimensionless gate charge of the SCB. In the transmon regime the spectrum is well approximated by

$$\omega_k(n_\mathrm{g}) = \omega_k(n_\mathrm{g} = 1/4) - \frac{\epsilon_k}{2}\cos(2\pi n_\mathrm{g}), \tag{37}$$

where

$$\epsilon_k \simeq (-1)^k E_\mathrm{C}\frac{2^{4k+5}}{k!}\sqrt{\frac{2}{\pi}}\left(\frac{E_\mathrm{J}}{2E_\mathrm{C}}\right)^{\frac{k}{2}+\frac{3}{4}} \mathrm{e}^{-\sqrt{8E_\mathrm{J}/E_\mathrm{C}}}, \tag{38}$$

giving a maximum thermal pure dephasing rate (for $n_\mathrm{g} = \pm 1/4$) of

$$\max\Gamma_\phi^k = \kappa^2\frac{Z_0}{R_K}\frac{k_\mathrm{B}T}{\hbar}\frac{\pi^3}{8}\left|\frac{\epsilon_k}{E_\mathrm{C}}\right|^2. \tag{39}$$

Here, we also note that in addition to small-amplitude thermal charge noise there can also be a slow but large-amplitude charge drift. In some cases, the effect of this drift can be taken into account by averaging over the range of transition frequencies involved. In the transmon regime, for the transition from $|k\rangle$ to $|k+1\rangle$ this is given by $\epsilon_{k+1} - \epsilon_k \approx \epsilon_{k+1}$.

2.5. Coherent drive

In the next section, we will examine the scattering of coherent signals on the transmon in the two-level and three-level approximations. To include a coherent drive in the description, we take the input field $\Phi^\mathrm{in}(t)$ to consist of a classical part $\Phi_\mathrm{cl}^\mathrm{in}(t)$ on top of the thermal background. Deriving the master equation for this case, it turns out that (26) is modified by adding the following time-dependent term to the system Hamiltonian,

$$H_\mathrm{d}(t) = -2\sqrt{\frac{\gamma}{Z_0}}\dot{\Phi}_\mathrm{cl}^\mathrm{in}(t)X. \tag{40}$$

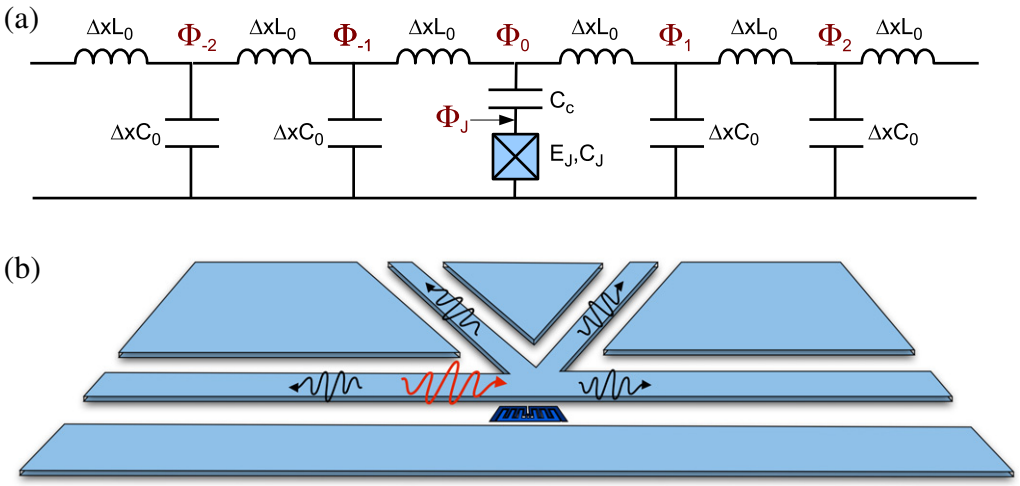

Figure 2. (a) Discretized circuit describing the interaction of an SCB with microwave photons propagating in an infinite TL. (b) Generalization of the input–output formalism to an arbitrary number of ports connected by an artificial atom.

2.6. Adding more transmission lines

In this section, we generalize the above master equation by adding more semi-infinite TLs to the SCB. First, by adding one more semi-infinite line, we arrive at the important case of an SCB capacitively coupled to an infinite TL. The discretized circuit is shown in figure 2(a), and the corresponding Hamiltonian is obtained from (1) by adding the TL terms for $x > 0$

$$H'_{\rm d} = H_{\rm d} + \frac{1}{\Delta x}\sum_{i>0}\left(\frac{p_i^2}{2C_0} + \frac{(\Phi_{i-1}-\Phi_i)^2}{2L_0}\right). \tag{41}$$

From a similar analysis as that above, we arrive at exactly the same master equation for the transmon's reduced density matrix, with the replacements

$$\Phi^{\rm in} = \frac{1}{2}\left(\Phi_{\rm L}^{\rm in} + \Phi_{\rm R}^{\rm in}\right), \quad \tau_{\rm RC} = \frac{Z_0}{2}\frac{C_{\rm c}C_{\rm J}}{C_\Sigma}, \ \gamma = \frac{Z_0}{2}\left(\frac{C_{\rm c}}{C_\Sigma}\right)^2 \tag{42}$$

and the output fields are obtained from

$$\Phi_{\rm L/R}^{\rm out} = \Phi_{\rm R/L}^{\rm in} + (\tau_{\rm RC}/C_{\rm J})p_{\rm J}. \tag{43}$$

We note that the damping constant γ as well as the RC time $\tau_{\rm RC}$ are both halved compared to the semi-infinite case, since the impedance to ground is halved to $Z_0/2$. The in-field is the sum of the fields incoming from the left and right, but compared to the semi-infinite case the coupling coefficient is halved, since there is (almost) no reflection at $x = 0$. Indeed, for a more general scenario with N symmetrically coupled incident fields, as illustrated in figure 2(b), the mapping would be

$$\Phi^{\rm in} = \frac{1}{N}\sum_{n=1}^{N}\Phi_n^{\rm in}, \quad \tau_{\rm RC} = \frac{Z_0}{N}\frac{C_{\rm c}C_{\rm J}}{C_\Sigma}, \quad \gamma = \frac{Z_0}{N}\left(\frac{C_{\rm c}}{C_\Sigma}\right)^2 \tag{44}$$

and using the relation $\Phi_0 = \Phi_n^{\text{in}} + \Phi_n^{\text{out}}$ $(\forall n)$, the output fields are given as

$$\Phi_n^{\text{out}} = \Phi_0 - \Phi_n^{\text{in}} = \left(\frac{2}{N} - 1\right)\Phi_n^{\text{in}} + \frac{\tau_{\text{RC}}}{C_{\text{J}}} p_{\text{J}} + \frac{2}{N}\sum_{m\neq n}^{N} \Phi_m^{\text{in}}. \tag{45}$$

3. Applications: scattering by the transmon

3.1. Two-level dynamics

In this section, we examine the scattering of coherent signals on the transmon in an open TL. The input field is a constant coherent signal with a single frequency ω_{p}, close to resonance with the first transition frequency ω_{10} of the transmon. Thus, we can safely describe the transmon as a two-level system. The master equation is given by (26) with a coherent drive and generalized to the case of an infinite TL (see sections 2.5 and 2.6), in the special case of only one system eigenfrequency ω_{10}. Moreover, we include an additional term due to pure dephasing, so that the total dephasing rates are given by (34). We represent our operators by the following Pauli matrices (using the notation $X_{ij} \equiv \langle i|X|j\rangle$):

$$H_{\text{sys}} = -\hbar\frac{\omega_{10}}{2}\sigma_z, \quad X^{\pm} = \pm \text{i}|X_{10}|\sigma^{\pm}. \tag{46}$$

Below, we will determine reflection and transmission coefficients for coherent signals scattered on the transmon. In the previous section, the incoming and outgoing fields were described in terms of the flux, since that gives a simpler description of the transmon. However, the voltage is a more intuitive quantity than the flux and is also usually what is measured in experiments. Therefore, in this section, we will describe the inputs and outputs in terms of the voltage.

We consider an incoming coherent voltage field,

$$V_{\text{L}}^{\text{in}}(t) = \Omega_p \sin\omega_{\text{p}} t, \tag{47}$$

impinging on the transmon from the left. For simplicity, we set the temperature to zero ($n_{\omega_{10}} = 0$). The reflected voltage field is the output to the left of the transmon. Using (42) and (43), we have

$$V_{\text{L}}^{\text{out}}(t) = -\sqrt{\frac{\gamma Z_0}{2}}\langle \dot{X}(t)\rangle, \tag{48}$$

where the expectation value can be written as

$$\langle \dot{X}(t)\rangle = \text{i}\omega_{10}\left(\langle X^{+}(t)\rangle - \langle X^{-}(t)\rangle\right) = -\omega_{10}|X_{10}|\langle\sigma^x\rangle. \tag{49}$$

Inserting (49) into (48) yields

$$V_{\text{L}}^{\text{out}}(t) = \frac{1}{2}\sqrt{\hbar\omega_{10}\Gamma_{10}Z_0}\langle\sigma^x\rangle = \sqrt{\hbar\omega_{10}\Gamma_{10}Z_0}Re\left[\rho_{01}\right], \tag{50}$$

where ρ_{01} is a density matrix element in the transmon eigenbasis.

To solve the master equation, we perform a unitary transformation to a frame rotating with the driving frequency ω_{p}. In this frame, the equation becomes time independent after employing the rotating-wave approximation. Solving the equation in the steady state ($\dot{\rho} = 0$) and transforming back to the non-rotaing frame yields the following expression for the desired density matrix element,

$$\rho_{01} = \frac{1}{2}\frac{\sqrt{\hbar\omega_{10}\Gamma_{10}Z_0}\left(\Delta + \text{i}\gamma_{10}\right)\Omega_p}{\hbar\omega_{10}Z_0\gamma_{10}^2 + \hbar\omega_{10}Z_0\Delta^2 + \gamma_{10}\Omega_{\text{p}}^2}\text{e}^{\text{i}\omega_{\text{p}}t}, \tag{51}$$

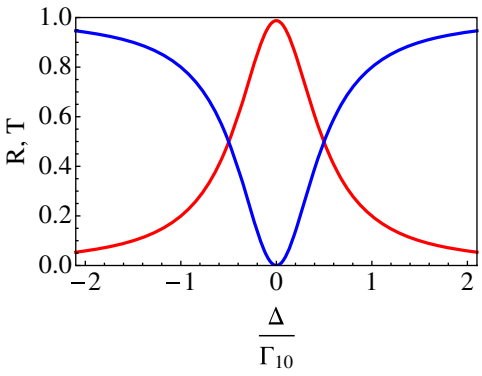

Figure 3. Reflectance R (red) and transmittance T (blue) for a two-level transmon as a function of detuning, with the average number of incoming photons per interaction time being $N_{\text{in}}/(\Gamma_{10}/2\pi) = 0.01$.

where $\Delta \equiv \omega_{\text{p}} - \omega_{10}$ is the detuning. Now, plugging this expression into (50) results in

$$V_{\text{L}}^{\text{out}}(t) = -\frac{\Omega_p}{2}\frac{\sin\omega_{\text{p}}t - \frac{\Delta}{\gamma_{10}}\cos\omega_{\text{p}}t}{\frac{\gamma_{10}}{\Gamma_{10}} + \frac{\Delta^2}{\Gamma_{10}\gamma_{10}} + 2\frac{N_{\text{in}},}{\Gamma_{10}}}, \tag{52}$$

where $N_{\text{in}} = \Omega_{\text{p}}^2/(2Z_0\hbar\omega_{10})$ is the average number of incoming photons per second. Thus, the reflection coefficient for the negative frequency part of the field is given by

$$r = -r_0\frac{1 - \text{i}\frac{\Delta}{\gamma_{10}}}{1 + \left(\frac{\Delta}{\gamma_{10}}\right)^2 + 2\frac{N_{\text{in}}}{\gamma_{10}}}, \tag{53}$$

with $r_0 \equiv \Gamma_{10}/2\gamma_{10}$. For the transmitted field, (43) yields

$$V_{\text{R}}^{\text{out}}(t) = V_{\text{L}}^{\text{in}}(t) - \sqrt{\frac{\gamma Z_0}{2}}\langle\dot{X}(t)\rangle \tag{54}$$

which directly gives us the following expression for the transmission coefficient:

$$t = 1 + r = \frac{1 - r_0 + \left(\frac{\Delta}{\gamma_{10}}\right)^2 + 2\frac{N_{\text{in}}}{\gamma_{10}} + \text{i}r_0\frac{\Delta}{\gamma_{10}}}{1 + \left(\frac{\Delta}{\gamma_{10}}\right)^2 + 2\frac{N_{\text{in}}}{\gamma_{10}}}. \tag{55}$$

In figure 3, we plot the reflectance $R = |r|^2$ and transmittance $T = |t|^2$ as a function of the detuning, in the case of a weak input signal and no pure dephasing. For a resonant drive ($\Delta = 0$), we see that perfect reflection is approached, in agreement with [12, 13, 39].

3.2. Three-level dynamics

In section 3.1, we showed that a low-amplitude input signal is totally reflected when it resonantly scatters off a transmon in the two-level approximation. In this section, we instead study the scattering off of a transmon in the three-level approximation. By strongly driving the second transition, the transmon becomes transparent to frequencies in resonance with the first

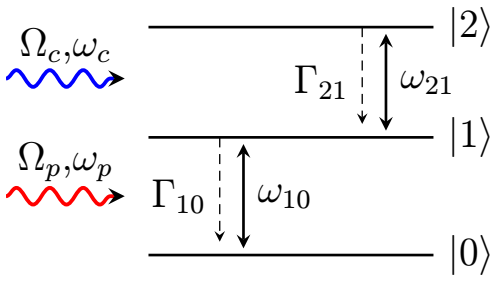

Figure 4. Internal levels of the transmon in the three-level approximation. A strong control field drives the $|1\rangle \rightarrow |2\rangle$ transition, rendering a transparency for the $|0\rangle \rightarrow |1\rangle$ transition.

transition. This effect is due to the Autler–Townes splitting and has been observed in recent experiments [22].

We consider an incoming voltage field from the left, consisting of a probe field $\Omega_\mathrm{p} \sin \omega_\mathrm{p} t$ close to resonance with the first transition (with detuning $\Delta_\mathrm{p} = \omega_\mathrm{p} - \omega_{10}$) and a control field $\Omega_\mathrm{c} \sin \omega_\mathrm{c} t$ close to resonance with the second transition (with detuning $\Delta_\mathrm{c} = \omega_\mathrm{c} - \omega_{21}$). Figure 4 shows the energy levels of the transmon in this approximation. In the transmon eigenbasis, the relevant operators are (with the ground state energy $\omega_0 = 0$)

$$H_\mathrm{sys} = \hbar \sum_{i=1}^{2} \omega_i \, |i\rangle \, \langle i| \,, \tag{56}$$

$$X = \mathrm{i} \sum_{i=1}^{2} |X_{i(i-1)}| (\sigma_i^+ - \sigma_i^-) \tag{57}$$

with $\sigma_i^+ = |i\rangle\langle i-1|$ and $\sigma_i^- = (\sigma_i^+)^\dagger$. In the same way as in the two-level case ((49)–(50)), we obtain the following expression for the reflected signal:

$$V_\mathrm{L}^\mathrm{out}(t) = -\sqrt{\frac{\gamma Z_0}{2}} \langle \dot{X}(t) \rangle = \frac{1}{2} \sum_{i=1}^{2} \sqrt{\hbar \omega_{i(i-1)} Z_0 \Gamma_{i(i-1)}} \langle \sigma_i^x \rangle, \tag{58}$$

with $\sigma_i^x = \sigma_i^+ + \sigma_i^-$. Thus, the reflected field consists of one part with frequencies around the probe frequency ω_p and one part with frequencies around the control frequency ω_c. Since we are interested in the reflectance and transmittance properties of the probe, we concentrate on the corresponding part of the reflected field

$$V_\mathrm{p}^\mathrm{ref}(t) = \frac{1}{2} \sqrt{\hbar \omega_{10} Z_0 \Gamma_{10}} \langle \sigma_1^x \rangle = \sqrt{\hbar \omega_{10} Z_0 \Gamma_{10}} Re(\rho_{10}). \tag{59}$$

The master equation is given by (26) for the case of two system eigenfrequencies, again with a coherent drive and generalized to the case of an infinite TL (see sections 2.5 and 2.6). Also, terms accounting for pure dephasing are added. To transform the master equation into a time-independent picture, we use the following unitary transformation matrix,

$$U(t) = \begin{pmatrix} 1 & 0 & 0 \\ 0 & \mathrm{e}^{-\mathrm{i}\omega_\mathrm{p} t} & 0 \\ 0 & 0 & \mathrm{e}^{-\mathrm{i}(\omega_\mathrm{p} + \omega_\mathrm{c}) t} \end{pmatrix} \tag{60}$$

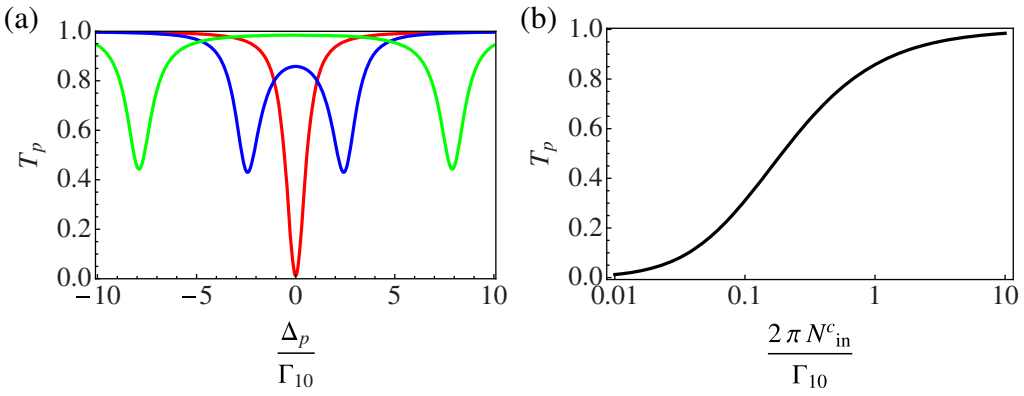

Figure 5. (a) Transmittance $T_{\rm p}$ of the probe as a function of detuning for three different control field strengths: $N^{\rm c}_{\rm in}/(\Gamma_{10}/(2\pi)) = 0.01$ (red), $N^{\rm c}_{\rm in}/(\Gamma_{10}/(2\pi)) = 1$ (blue) and $N^{\rm c}_{\rm in}/(\Gamma_{10}/(2\pi)) = 8$ (green). (b) Transmittance as a function of the control field strength for a resonant probe field ($\Delta_{\rm p} = 0$).

and employ the rotating-wave approximation. As before, we solve the master equation in the steady state to determine ρ_{10}, but we now consider two different cases.

Firstly, by setting $\Omega_{\rm c} = 0$, we recover exactly the same expression for the reflected field as in the two-level case. Thus, with the control field turned off, we see almost full reflection for weak probe fields in resonance with the first transition frequency of the transmon.

Secondly, we consider the case of a strong control field ($\Omega_{\rm c} \gg \Omega_{\rm p}$). Solving the master equation and expanding ρ_{10} to first order in $(\Omega_{\rm p}/\Omega_{\rm c})$, we obtain the following expression:

$$\rho^{(1)}_{10} = -\frac{2{\rm i}\hbar\omega_{21} Z_0 \sqrt{\frac{\Gamma_{10}}{\hbar\omega_{10} Z_0}} \left(\gamma_{20} - {\rm i}\left(\Delta_{\rm c} + \Delta_{\rm p}\right)\right) \Omega_{\rm p}}{4\hbar\omega_{21} Z_0 \left(\gamma_{10} - {\rm i}\Delta_p\right) \left(\gamma_{20} - {\rm i}\left(\Delta_{\rm c} + \Delta_{\rm p}\right)\right) + \Gamma_{21}\Omega_{\rm c}^2} {\rm e}^{-{\rm i}\omega_{\rm p} t}. \tag{61}$$

Inserting (61) into (59), we can determine the reflection coefficient. For a resonant control field ($\Delta_{\rm c} = 0$), the result is

$$r = -\frac{2\Gamma_{10}\left(\gamma_{20}^2 + \Delta_{\rm p}^2\right)\left(\gamma_{10} - {\rm i}\Delta_{\rm p}\right) + \Gamma_{10}\Gamma_{21}\left(\gamma_{20} + {\rm i}\Delta_{\rm p}\right) N^{\rm c}_{\rm in}}{4\left(\gamma_{10}^2 + \Delta_{\rm p}^2\right)\left(\gamma_{20}^2 + \Delta_{\rm p}^2\right) + 4\Gamma_{21}\left(\gamma_{10}\gamma_{20} - \Delta_{\rm p}^2\right) N^{\rm c}_{\rm in} + \Gamma_{21}^2 N^{\rm c2}_{\rm in}}, \tag{62}$$

where $N^{\rm c}_{\rm in} = \Omega_{\rm c}^2/(2Z_0\hbar\omega_{21})$ is the average number of incoming photons per second in the control field. The transmission coefficient is again given by $t = 1 + r$. Figure 5 shows the transmittance $T = |t|^2$ for different probe detunings and control field strengths. In these plots, we have neglected pure dephasing and used (29) to express Γ_{21} in terms of Γ_{10}.

We can clearly see that, for strong control fields, the transmittance of a resonant probe approaches unity. Thus, by turning on and off a strong resonant control field, we can switch between the cases of full transmission and full reflection for the resonant probe.

3.3. Second-order correlations

In a recent experiment [23], the second-order statistics of the field scattered off a transmon was measured. In this section, inspired by the experiment, we analyze the second-order correlation

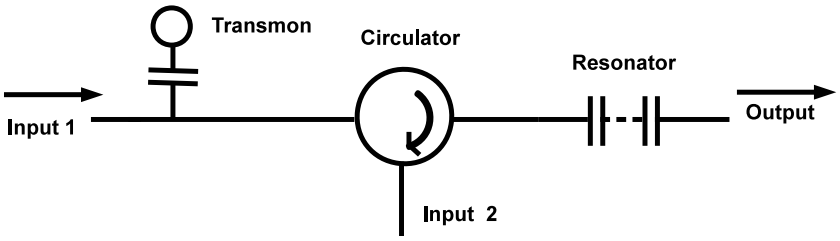

Figure 6. Schematic model of a transmon cascaded with a resonator. The circulator prevents the field reflected from the resonator to reach the transmon. Using input port 1 (2), the output is the filtered transmitted (reflected) signal.

functions in our system. The normalized second-order correlation function is in the steady state given as [40]

$$g^{(2)}(\tau) = \frac{\langle V^+(t)V^+(t+\tau)V^-(t+\tau)V^-(t)\rangle}{\langle V^+(t)V^-(t)\rangle^2} \tag{63}$$

and is proportional to the conditional probability of detecting a photon at time $t+\tau$, given that one was detected at time t. Here, $V^{\pm}(t)$ are the positive and negative frequency parts of the voltage field.

We calculate $g^{(2)}(\tau)$ for the transmitted and reflected fields from a transmon driven by a resonant coherent signal. We treat the transmon as a two-level system and use the same notation as in section 3.1. To be able to compare with the experiments in [23], we perform the calculations for finite temperatures and a finite detection bandwidth on the output signal. For zero temperature and infinite bandwidth, we recover the results of [41]: perfect antibunching in the reflected field and bunching in the transmitted field.

Including the effect of a finite detection bandwidth is straighforward by including a filter in the calculations. The approach we have taken is to model the filter by a single-mode TL resonator in resonance with the transmon, with the Hamiltonian

$$H_{\rm res} = \hbar\omega_{10} a^\dagger a \tag{64}$$

and cascade it with the transmon. We start from the QLE (22) for the transmon, generalized to the case of an infinite TL (see section 2.6), and a similar equation for the resonator. Our coherent input signal is the voltage field $V_{\rm L}^{\rm in}(t) = \Omega_{\rm d} \sin\omega_{\rm d} t$, just like in section 3.1. We can then use the formalism of cascaded quantum systems in [34] to arrive at a master equation for the joint density matrix of the transmon and the resonator. In this formalism, the output from the transmon (reflected or transmitted) is taken as input to the resonator, without any signals going the opposite way (see figure 6). For the field reflected from the transmon, the resulting master equation is

$$\begin{aligned}\dot\rho = {} & \frac{\rm i}{\hbar}[\rho, H_{\rm sys}+H_{\rm res}] + \Gamma_{10}\mathcal{D}(\sigma^-)\rho + \Gamma_{01}\mathcal{D}(\sigma^+)\rho + \gamma_{\rm BW}\left[\left(\frac{n_{\omega_{10}}}{2}+1\right)\mathcal{D}(a)\rho + \frac{n_{\omega_{10}}}{2}\mathcal{D}(a^\dagger)\rho\right] \\ & + \frac{1}{2}{\rm i}\sqrt{\Gamma_{10}(n_{\omega_{10}}+1)\gamma_{\rm BW}}\left([a,\rho\sigma^+]+[a^\dagger,\sigma^-\rho]\right) \\ & + \frac{1}{2}{\rm i}\sqrt{\Gamma_{01}n_{\omega_{10}}\gamma_{\rm BW}}\left([\sigma^+\rho,a]+[\rho\sigma^-,a^\dagger]\right) + {\rm i}\sqrt{\frac{\Gamma_{10}N_{\rm in}}{2(n_{\omega_{10}}+1)}}[\rho,\sigma^x],\end{aligned} \tag{65}$$

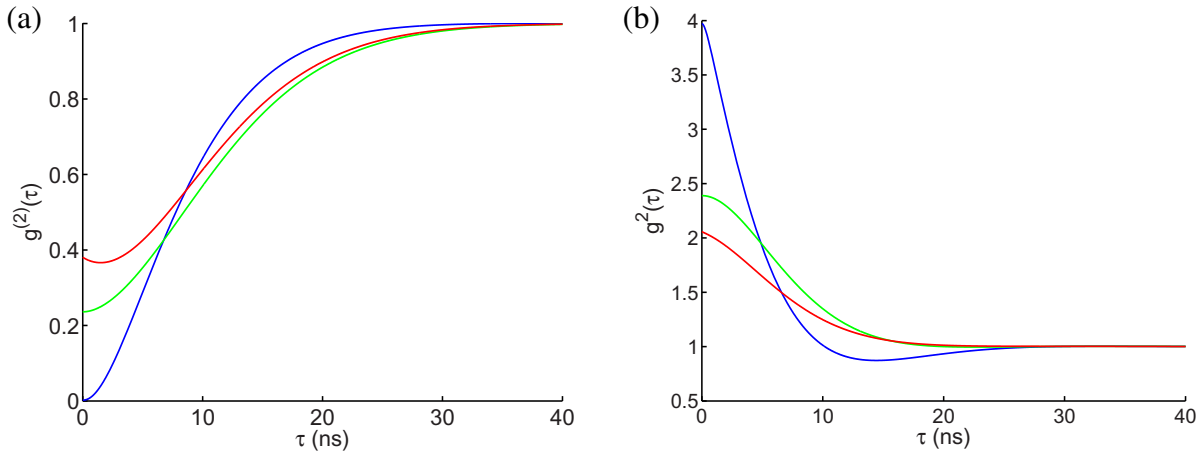

Figure 7. $g^{(2)}(\tau)$ for the fields reflected from and transmitted through a transmon for different temperatures and detection bandwidths. Typical parameter values from recent experiments are used ($\Gamma_{10}/2\pi = 41$ MHz, $\omega_{10}/2\pi = 5.12$ GHz). (a) Reflected field: blue ($T = 0$, BW $= 1$ GHz), green ($T = 0$, BW $= 55$ MHz), red ($T = 50$ mK, BW $= 55$ MHz), with $P = -131$ dBm. (b) Transmitted field: blue ($T = 0$, BW $= 1$ GHz), green ($T = 0$, BW $= 55$ MHz), red ($T = 80$ mK, BW $= 55$ MHz), with $P = -127$ dBm.

where we have denoted the filter bandwidth by γ_{BW}. For the field transmitted through the transmon, (65) is modified by simply adding the following term to the right-hand side:

$$\sqrt{\frac{\gamma_{\mathrm{BW}} N_{\mathrm{in}}}{2}}[\rho, a^\dagger - a]. \tag{66}$$

The output we are interested in is the voltage field leaking out at the right side of the resonator, whose positive and negative frequency parts are proportional to $a(t)$ and $a^\dagger(t)$, respectively. Thus, $g^{(2)}(\tau)$ can be calculated as

$$g^{(2)}(\tau) = \frac{\langle a^\dagger(t)a^\dagger(t+\tau)a(t+\tau)a(t)\rangle}{\langle a^\dagger(t)a(t)\rangle^2} = \frac{\mathrm{Tr}\left[a^\dagger a P(\tau)(a\rho_{\mathrm{s}}a^\dagger)\right]}{\mathrm{Tr}\left[a^\dagger a\rho_{\mathrm{s}}\right]^2}, \tag{67}$$

where ρ_{s} is the steady-state density matrix and $P(\tau)$ the propagator super-operator, defined by $\rho(t+\tau) = P(\tau)\rho(t)$. Both ρ_{s} and $P(\tau)$ are obtained by solving the master equations (65) and (66). For the case without filter, $g^{(2)}(\tau)$ for the reflected field is given by (67) with a replaced by σ^-. Since $(\sigma^-)^2 = 0$, it directly follows that $g^{(2)}(0) = 0$, i.e. perfect antibunching.

In figure 7(a), we plot $g^{(2)}(\tau)$ for the reflected field for different temperatures and detection bandwidths. Typical parameter values from recent experiments [23] are used. For zero temperature and large bandwidth we see perfect antibunching, as expected. For a decreased bandwidth the full time dynamics of the antibunching cannot be resolved, which results in a less pronounced antibunching dip. For finite temperatures, we see even less antibunching, due to a nonzero probability of detecting bunched thermal photons. In figure 7(b), we plot $g^{(2)}(\tau)$ for the transmitted field for different temperatures and detection bandwidths. Here we see a decrease of the superbunching for higher temperatures and smaller bandwidths. These results explain the qualitative features of the experimental data in [23] well.

4. Summary and conclusions

Summing up, we have performed a thorough analysis of the qubit–photon scattering in a one-dimensional continuum from a microscopic point of view. In particular, we have derived a master equation description using a superconducting transmon qubit as our scatterer. When we consider the two lowest levels of the transmon, it behaves like a mirror for the incoming photons. Then, going beyond to the two-level approximation, we can use a control field resonant with a second transition of the transmon to suppress this reflection of photons at the probe frequency. Finally, we discussed how the photon antibunching observed in the reflected field is reduced by finite temperature and finite detection bandwidth.

Acknowledgments

We thank T Willemen and Tauno Palomaki for valuable discussions. We acknowledge financial support from the Swedish Research Council, the Wallenberg Foundation, the STINT and from the EU through the ERC and the projects SOLID and PROMISCE. This work was also supported by the Spanish MICINN project FIS2009-10061 and the CAM research consortium QUITEMAD S2009-ESP-1594. BP acknowledges support from the CSIC grant JAE-PREDOC2009.

References

[1] Clarke J and Wilhelm F K 2008 Superconducting quantum bits *Nature* **453** 1031–42
[2] Schoelkopf R J and Girvin S M 2008 Wiring up quantum systems *Nature* **451** 664–9
[3] Blais A, Huang R-S, Wallraff A, Girvin S M and Schoelkopf R J 2004 Cavity quantum electrodynamics for superconducting electrical circuits: an architecture for quantum computation *Phys. Rev.* A **69** 062320
[4] Wallraff A, Schuster D I, Blais A, Frunzio L, Huang R-S, Majer J, Kumar S, Girvin S M and Schoelkopf R J 2004 Strong coupling of a single photon to a superconducting qubit using circuit quantum electrodynamics *Nature* **431** 162–7
[5] Schuster D I, Wallraff A, Blais A, Frunzio L, Huang R-S, Majer J, Girvin S M and Schoelkopf R J 2005 ac Stark shift and dephasing of a superconducting qubit strongly coupled to a cavity field *Phys. Rev. Lett.* **94** 123602
[6] Schuster D I *et al* 2007 Resolving photon number states in a superconducting circuit *Nature* **445** 515–8
[7] Majer J *et al* 2007 Coupling superconducting qubits via a cavity bus *Nature* **449** 443–7
[8] Houck A A *et al* 2007 Generating single microwave photons in a circuit *Nature* **449** 328–31
[9] Fink J M, Göppl M, Baur M, Bianchetti R, Leek P J, Blais A and Wallraff A 2008 Climbing the Jaynes–Cummings ladder and observing its nonlinearity in a cavity QED system *Nature* **454** 315–8
[10] Karyn Le Hur 2012 Kondo resonance of a microwave photon *Phys. Rev.* B **85** 140506
[11] Knill E, Laflamme R and Milburn G J 2001 A scheme for efficient quantum computation with linear optics *Nature* **409** 46–52
[12] Shen J-T and Fan S 2005 Coherent single photon transport in a one-dimensional waveguide coupled with superconducting quantum bits *Phys. Rev. Lett.* **95** 213001
[13] Shen J T and Fan S 2005 Coherent photon transport from spontaneous emission in one-dimensional waveguides *Opt. Lett.* **30** 2001–3
[14] Micheli A and Zoller P 2006 Single-atom mirror for one-dimensional atomic lattice gases *Phys. Rev.* A **73** 043613
[15] Zheng H, Gauthier D J and Baranger H U 2010 Waveguide QED: many-body bound-state effects in coherent and Fock-state scattering from a two-level system *Phys. Rev.* A **82** 063816

[16] Zheng H, Gauthier D J and Baranger H U 2012 Strongly correlated photons generated by coupling a three- or four-level system to a waveguide *Phys. Rev.* A **85** 043832
[17] Kocabaş S E, Rephaeli E and Fan S 2012 Resonance fluorescence in a waveguide geometry *Phys. Rev.* A **85** 023817
[18] Astafiev O, Zagoskin A M, Abdumalikov A A, Pashkin Yu A, Yamamoto T, Inomata K, Nakamura Y and Tsai J S 2010 Resonance fluorescence of a single artificial atom *Science* **327** 840–3
[19] Astafiev O V, Abdumalikov A A, Zagoskin A M, Pashkin Yu A, Nakamura Y and Tsai J S 2010 Ultimate on-chip quantum amplifier *Phys. Rev. Lett.* **104** 183603
[20] Abdumalikov A A, Astafiev O, Zagoskin A M, Pashkin Yu A, Nakamura Y and Tsai J S 2010 Electromagnetically induced transparency on a single artificial atom *Phys. Rev. Lett.* **104** 193601
[21] Abdumalikov A A, Astafiev O V, Pashkin Yu A, Nakamura Y and Tsai J S 2011 Dynamics of coherent and incoherent emission from an artificial atom in a 1D space *Phys. Rev. Lett.* **107** 043604
[22] Hoi I-C, Wilson C M, Johansson G, Palomaki T, Peropadre B and Delsing P 2011 Demonstration of a single-photon router in the microwave regime *Phys. Rev. Lett.* **107** 073601
[23] Hoi I-C, Palomaki T, Lindkvist J, Johansson G, Delsing P and Wilson C M 2012 Generation of nonclassical microwave states using an artificial atom in 1D open space *Phys. Rev. Lett.* **108** 263601
[24] Hoi I-C, Wilson C M, Johansson G, Palomaki T, Stace T M, Fan B and Delsing P 2012 Giant cross Kerr effect for propagating microwaves induced by an artificial atom arXiv:1207.1203
[25] Hoi I-C, Wilson C M, Johansson G, Lindkvist J, Peropadre B, Palomaki T and Delsing P 2013 Microwave quantum optics with an artificial atom in one-dimensional open space *New J. Phys.* **15** 025011
[26] Bouchiat V, Vion D, Joyez P, Esteve D and Devoret M H 1998 Quantum coherence with a single Cooper pair *Phys. Scr.* **T76** 165–70
[27] Nakamura Y, Pashkin Y A and Tsai J S 1999 Coherent control of macroscopic quantum states in a single Cooper-pair box *Nature* **398** 786–8
[28] Makhlin Y, Schön G and Shnirman A 2001 Quantum-state engineering with Josephson-junction devices *Rev. Mod. Phys.* **73** 357–400
[29] Lehnert K W, Bladh K, Spietz L F, Gunnarsson D, Schuster D I, Delsing P and Schoelkopf R J 2003 Measurement of the excited-state lifetime of a microelectronic circuit *Phys. Rev. Lett.* **90** 027002
[30] Bladh K, Duty T, Gunnarsson D and Delsing P 2005 The single Cooper-pair box as a charge qubit *New J. Phys.* **7** 180
[31] Büttiker M 1987 Zero-current persistent potential drop across small-capacitance Josephson junctions *Phys. Rev.* B **36** 3548–55
[32] Duty T, Gunnarsson D, Bladh K and Delsing P 2004 Coherent dynamics of a Josephson charge qubit *Phys. Rev.* B **69** 140503
[33] Koch J, Yu T M, Gambetta J, Houck A A, Schuster D I, Majer J, Blais A, Devoret M H, Girvin S M and Schoelkopf R J 2007 Charge-insensitive qubit design derived from the Cooper pair box *Phys. Rev.* A **76** 042319
[34] Gardiner C W and Zoller P 1991 *Quantum Noise* (Berlin: Springer)
[35] Yurke B and Denker J S 1984 Quantum network theory *Phys. Rev.* A **29** 1419–37
[36] Devoret M H 1997 Quantum fluctuations in electrical circuits *Quantum Fluctuations* (*Les Houches Session LXIII*) (Amsterdam: Elsevier) pp 351–86
[37] Johansson G, Tornberg L, Shumeiko V S and Wendin G 2006 Readout methods and devices for Josephson-junction-based solid-state qubits *J. Phys.: Condens. Matter* **18** S901
[38] Rau I, Johansson G and Shnirman A 2004 Cavity quantum electrodynamics in superconducting circuits: susceptibility at elevated temperatures *Phys. Rev.* B **70** 054521
[39] Romero G, García-Ripoll J J and Solano E 2009 Microwave photon detector in circuit QED *Phys. Rev. Lett.* **102** 173602
[40] Gerry C C and Knight P L 2005 *Introductory Quantum Optics* (Cambridge: Cambridge University Press)
[41] Chang D E, Sørensen A S, Demler E A and Lukin M D 2007 A single-photon transistor using nanoscale surface plasmons *Nature Phys.* **3** 807–12